



Search for Anomalous Production of $\gamma + b + j + \cancel{E}_T + X$

The CDF Collaboration
URL <http://www-cdf.fnal.gov>
(Dated: April 18, 2008)

We present a search for anomalies in events with a photon, at least one secondary vertex (SECVTX) tag, 2^{nd} jet, and \cancel{E}_T at $\sqrt{s} = 1.96$ TeV. Our search uses data corresponding to 2 fb^{-1} of integrated luminosity collected between February 2002 and May 2007. We report observed event counts, Standard Model background predictions, and kinematic distributions. We find no indications of anomalous production in this final state.

Preliminary Results Spring 2008

I. INTRODUCTION

In this note we describe a search for new physics in the $\gamma + b + j + \cancel{E}_T$ channel. The original motivation for looking at this signature was following up a model of supersymmetry breaking in which a photino radiatively decays via a loop into a Higgsino LSP [1], which had been motivated by the recording of the CDF $ee\gamma\gamma\cancel{E}_t$ event [2]. In this model the production of a chargino and a neutralino could result in a final state with the signature of a high photon accompanied by b -quark and a c -quark, and missing transverse momentum, via the decay chain:

$$\tilde{\chi}_1^+ \tilde{\chi}_2^0 \rightarrow (\bar{b}t)(\gamma\tilde{\chi}_1^0) \rightarrow (\bar{b}c\tilde{\chi}_1^0)(\gamma\tilde{\chi}_1^0) \rightarrow (\gamma\bar{b}c\cancel{E}_T) \quad (1)$$

There has also been interest in Technicolor models in similar signatures, but without \cancel{E}_T ; K. Lane, in particular, has pointed to these photon channels as possibly very exciting [3]. Other, related, signatures are discussed in Refs. [4] and [5].

Finally, it is interesting to note that it is very difficult to create a final state containing a photon, b -jet, and \cancel{E}_T in the Standard Model. The main background in this final state will come from events where mismeasurements of the jet energy induce transverse missing energy which is not associated with unobserved neutral particles. If we aggressively reduce the amount of mismeasurement of the \cancel{E}_T we will be left with relatively few background events. This final state, therefore, provides us with an excellent place to look for new phenomena effects that are produced with relatively small cross sections.

II. EVENT SELECTION

This analysis is based on a dataset corresponding to an integrated luminosity of 2.0 fb^{-1} collected with the CDF II detector [6] between February 2002 and May 2007. The data are collected using a trigger that requires a high energy, isolated cluster in the central portion of the electromagnetic calorimeter. This preselection provides a dataset enhanced with high energy central photons.

The offline selections require a photon, 2 jets, one of which is b -tagged, and missing transverse energy. We reject events with a primary vertex outside the interaction region, $|z| > 60 \text{ cm}$. The photon is required to have $|\eta| < 1.1$, where the pseudorapidity $\eta = -\ln[\tan(\theta/2)]$, and transverse energy $E_T > 25 \text{ GeV}$. Note that θ is measured with respect to the origin of the detector coordinate system and not the coordinate system associated with the interaction vertex. Jets are reconstructed using a cone algorithm with radius $\Delta R = \sqrt{\Delta\phi^2 + \Delta\eta^2} = 0.4$ and the jet energies are corrected for calorimeter response and multiple interactions. These corrected jets are required to have $|\eta| < 2$ and $E_T > 15 \text{ GeV}$. At least one of the jets must be tagged as a b -jet using the SECVTX algorithm [7], which searches for displaced vertices using the tracks inside the jet cone. We correct the raw measured missing transverse energy for the presence of photons, electrons, muons, and jets in the event and then require this corrected \cancel{E}_T to be greater than 25 GeV . We minimize the effect of mismeasured jets on the calculation of the \cancel{E}_T by requiring the difference in azimuthal angle between any jet and the \cancel{E}_T , $\Delta\phi(\text{jet}, \cancel{E}_T)$, to be greater than 0.3 . The final requirement is that ΔR between the two leading jets as well as between each of the two jets and the photon must be greater than 0.4 . Table II summarizes the effects of the event selections on the signal sample.

Cut	Number passing
Standard $\gamma + 2$ jets	1944962
$\Delta R > 0.4$ and $\cancel{E}_T \geq 25$	35463
$\Delta\phi(\text{jet} \rightarrow \cancel{E}_T)$	18128
≥ 1 tight tag	617

TABLE I: Summary of event selections. Note that the first selection, ‘‘Standard $\gamma + 2$ jets’’, includes the trigger, z -vertex cuts, $E_T(\gamma)$, and $E_T(\text{jets})$ as described in Section II.

III. BACKGROUND PREDICTIONS

There were four very general backgrounds that we attempted to estimate: we looked at background events with real and fake b -tags and with real and fake photons. Table III summarizes our four main backgrounds.

Background A was estimated by generating Monte Carlo events using MadGraph [8] for the matrix element process and Pythia [9] for parton showering and hadronization. A CKKW matching scheme [10] has been implemented to avoid double-counting QCD radiation. For this background, we generate separate $\gamma + b +$ jets and $\gamma + c +$ jets samples.

	Real Photon	Fake Photon
Real b-tag	A	B
Fake b-tag	C	D

TABLE II: Summary of backgrounds

Backgrounds B and D (fake photon) were estimated from the data sample itself by using cluster shape variables from the shower maximum detector and hit rates in the preradiator [11]. This technique, called the “*CES/CP2* method”, allows us to determine the fraction of photons in our sample that are being faked by jets. We describe it in more detail in Sec. III A.

Background C (real photon, fake b -tag) was estimated by selecting events that passed all cuts except “at least one tagged jet” and then applying a parametrization of the tagging rate that uses jet E_T , the number of tracks in the jet, jet η , jet ϕ , and the total scalar sum of the E_T of all the jets. These parameterizations are termed *tag matrices* [7]. The matrix determined from events having negative values of transverse decay length, $l_{2d} < 0$, also called the *mistag matrix*, is used to determine the number of fake b -tags. After this determination, we obtain the real photon contribution of the mistagged sample by applying the CES/CP2 method.

The normalizations and shapes of backgrounds B, C, and D are obtained directly from the CES/CP2 method and mistag matrix. The shapes of the contributions from background A are obtained from the MC samples after matching is applied. The normalization of these backgrounds is obtained through fitting the secondary vertex mass distribution of the tagged jets, $m(SV)$, to templates. This normalization scheme is described in Sec. IV.

A. Fake Photon Fraction

As mentioned above, we use the CES/CP2 technique to estimate the real and fake photon contributions. We briefly describe the method in this section. The primary background to events with a real single photon comes from meson decays to diphotons, for example $\pi^0 \rightarrow \gamma\gamma$. For photon candidates with $E_T < 35$ GeV, we use the shape of the shower profile to discriminate between real single photon events and diphoton final states from decays of mesons. We construct a χ^2 by comparing the measured shower profile with that from electron test beam data. A real single photon has an average probability of $\sim 78\%$ to satisfy a χ^2 cut, while the background has an average probability of $\sim 30\%$, since the shower profile of the two near-by photons from a meson decay is measurably wider on average.

Above 35 GeV, however, the two photons from meson decay coalesce and the discrimination power of the shower profile measurement is lost. In this E_T range, we use hit rates in the preshower detector to discriminate between real single photons and diphoton showers from meson decays. A single photon will convert and leave a hit in the preshower detector with a probability of $\sim 65\%$. Backgrounds that decay into two photons have a hit probability of $\sim 85\%$ because the probability that neither photon converts is lower than the probability that a single photon doesn’t convert. The difference of probabilities between signal and background forms the basis of a statistical method which assigns each event a weight for being a real photon. The weight is computed based on the energy of the photon candidate, the angle of incidence, the number of primary interactions found in the event, the shower profile χ^2 , and whether or not the photon candidate leaves a hit in the preshower detector.

Utilizing this technique, we estimate the true photon fraction in the signal region to be,

$$f(\text{real } \gamma) = 0.81 \pm 0.08 \text{ (stat.)} \pm 0.09 \text{ (syst.)}. \quad (2)$$

IV. HEAVY FLAVOR NORMALIZATION

The invariant mass of the tracks that form a secondary vertex, used to “tag” the event, can be used to discriminate between the bottom, charm, and light species that make up the sample. We use this discriminating power to normalize the contributions of real heavy flavor + real photon, background D in Table III, by fitting the secondary vertex mass distribution. Because the photon couples to charge and may thereby alter the heavy flavor fraction and the event topology of photon events may be different from those of generic heavy flavor or QCD, we use templates that are derived from samples containing real photons.

The three templates we use are listed below.

- The bottom template is obtained from the MadGraph $\gamma + b$ sample.
- The charm template is obtained from the MadGraph $\gamma + c$ sample.

- The light template is obtained from a Pythia inclusive photon sample.

Figure 1 shows the three templates normalized to unit area and overlaid on the same plot, highlighting the discriminating power of this variable. The feature in the charm template near $m(SV) = 1.8 \text{ GeV}/c^2$ is attributable to D^0 and D^+ decays where the invariant mass of the constituent tracks almost reproduces the decaying hadron. This peak is prominent because the D^0 and D^+ hadrons are the most common components of charm jets. We perform a binned maximum likelihood fit to the templates using the package *RooFit* [12].

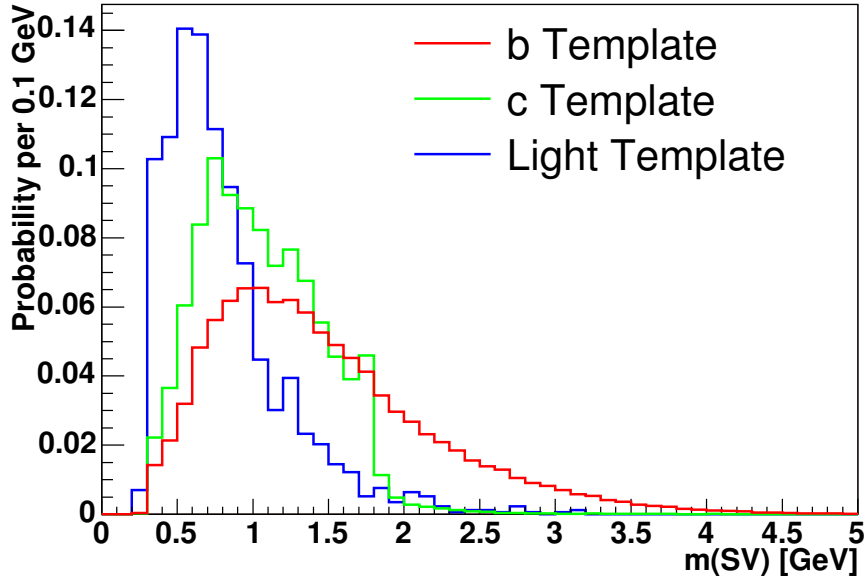


FIG. 1: Bottom, charm, and light templates normalized to unit area.

The standard photon sample has some contribution from jets faking photons, as described in Sec. III. Because we need to normalize the *real* photon + heavy flavor samples, we must subtract the fake photon contribution to the heavy flavor fraction. This is accomplished by fitting two distributions, the standard photon sample and a sample enriched with jets faking photons, referred to as the *loose* photon sample. We subtract the contribution of fake photons to the heavy flavor fraction by using the CES/CP2 fake photon fraction as seen in equation 3.

$$f_{\text{heavy}}^{\text{real } \gamma} = f_{\text{heavy}}^{\text{standard } \gamma} - f_{\text{CES/CP2}}^{\text{fake}} \cdot f_{\text{heavy}}^{\text{loose } \gamma}. \quad (3)$$

We normalize both the charm and bottom contributions using equation 3 but the technique is slightly different for the two types of heavy quarks. First, we describe the normalization of the bottom component.

The bottom contribution is normalized by fitting a “control” region, defined as $\gamma + b$ -tag, and then extrapolating to the signal region by using efficiencies derived from the $\gamma + b$ Monte Carlo. The necessary efficiencies are,

- $\varepsilon(N_{\text{jet}} \geq 2)$: defined as the ratio of the number of events containing 2 or more jets to the number of events containing 1 or more jets satisfying our jet selection.
- $\varepsilon(\cancel{E}_T)$: defined as the ratio of the number of events containing $\cancel{E}_T > 25 \text{ GeV}$ with 2 or more jets to the number containing 2 or more jets.
- $\varepsilon(\cancel{E}_T \text{ clean})$: defined as the ratio of the number of events satisfying $\Delta\phi(\text{jet} \rightarrow \cancel{E}_T)$ to the number of events satisfying $\cancel{E}_T > 25 \text{ GeV}$ and two jets.

These efficiencies are found to be $\varepsilon(N_{\text{jet}} \geq 2) = 0.717 \pm 0.003$, $\varepsilon(\cancel{E}_T) = 0.066 \pm 0.002$, and $\varepsilon(\cancel{E}_T \text{ clean}) = 0.26 \pm 0.01$. The final efficiency that takes us from the control to the signal region is therefore,

$$\varepsilon(\text{final}) = \varepsilon(N_{\text{jet}} \geq 2) \cdot \varepsilon(\cancel{E}_T) \cdot \varepsilon(\cancel{E}_T \text{ clean}) = 0.01230 \pm 0.00001. \quad (4)$$

Figures 2 and 3 show the secondary vertex mass fits to the control region. After applying equation 3, we obtain $f_b(\text{control}) = 0.297 \pm 0.005$ (stat.) ± 0.040 (CES/CP2). We then apply equation 4 to obtain a prediction for the fraction of real $\gamma + \text{real } b$ events in our signal region of,

$$f_b(\text{predicted}) = 0.47 \pm 0.02 \text{ (stat.)} \pm 0.06 \text{ (CES/CP2)} \quad (5)$$

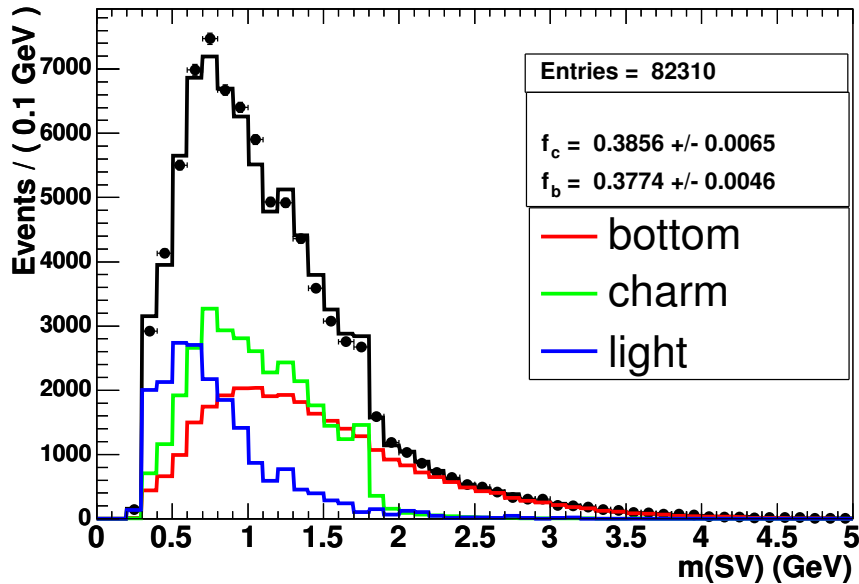


FIG. 2: Secondary vertex mass fit in the control sample, $\gamma + b + X$, using standard photons.

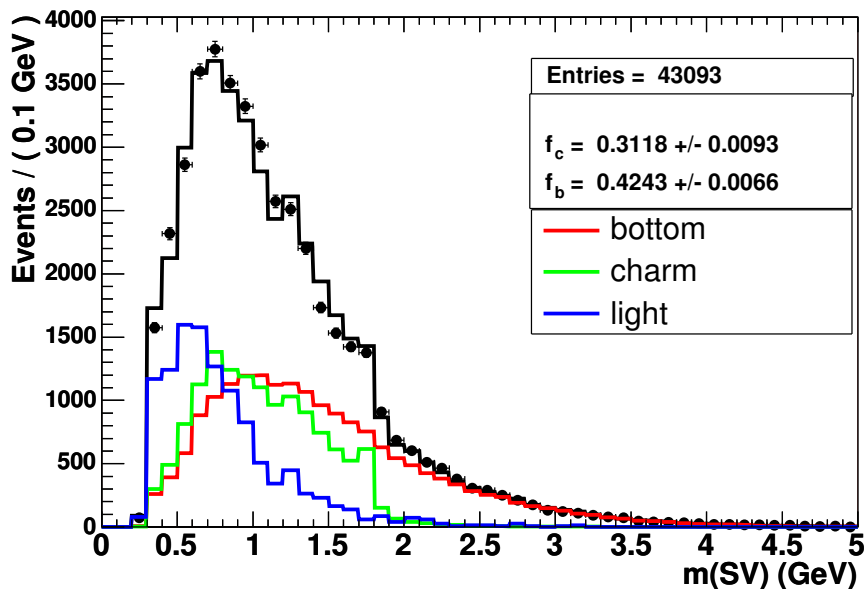


FIG. 3: Secondary vertex mass fit in the control sample, $\gamma + b + X$, using loose photons.

The charm sample is normalized by directly fitting secondary vertex mass in the signal region. We do not extrapolate the charm normalization from the control sample because the uncertainties on the matching scheme for charm are

large. Figures 4 and 5 show the fits to the signal sample using standard and loose photons, respectively. Using equation 3 we obtain,

$$f_c(\text{signal}) = 0.15 \pm 0.08 \text{ (stat.)} \pm 0.01 \text{ (CES/CP2)} \quad (6)$$

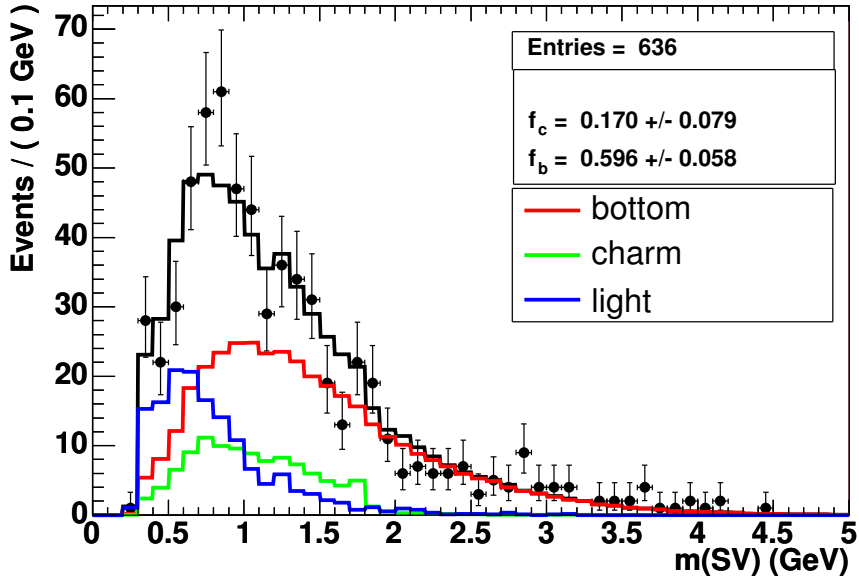


FIG. 4: Secondary vertex mass fit in the signal sample using standard photons.

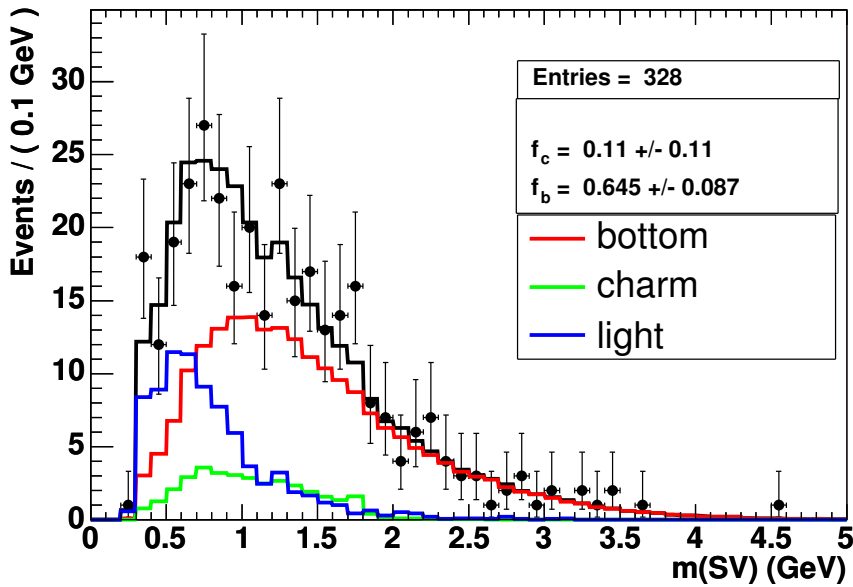


FIG. 5: Secondary vertex mass fit in the signal sample using loose photons.

As a cross-check of the extrapolation procedure for the bottom normalization, we also show the result of the direct fit to the signal region for the bottom fraction below,

$$f_b(\text{direct}) = 0.47 \pm 0.06 \text{ (stat.)} \pm 0.06 \text{ (CES/CP2)}. \quad (7)$$

The predicted bottom fraction agrees well with the direct fit.

V. SYSTEMATIC UNCERTAINTIES

Sources of systematic uncertainty include errors coming from the estimation of the real photon fraction, the application of the mistag matrix, and the variation in template shapes used in the secondary vertex mass fit.

A. Real Photon Fraction

Systematic uncertainties on the real and fake photon fraction estimates arise from variations in the values of the preshower hit rate, the rate of backscattered showers, and the fractional composition of fake photon backgrounds.

B. Mistag Rate

The uncertainty on the mistag matrix prediction for the rate of mistagged light jets is estimated to be 15% [7].

C. Template Shape Variation

We estimate a systematic uncertainty arising from the secondary vertex mass fitting procedure by varying the shapes of the templates which are used in the binned likelihood fit. The systematic effect of mismodeled tracking inefficiency in the Monte Carlo is estimated by shifting the secondary vertex mass templates down by 3%. We also refit the secondary vertex mass distributions with templates derived from samples that have the $\cancel{E}_T > 25$ GeV cut imposed on them, as this may change the relative fraction of semileptonic decays in our template samples and thereby alter the secondary vertex mass distribution. Because both of these sources of uncertainty affect the shape of the templates, we take the maximum variation observed as our systematic shift in normalization.

VI. RESULTS

Table VI summarizes the contributions to the background with associated statistical and systematic uncertainties. The total background prediction is

$$N(\text{predicted BG}) = 637 \pm 54 (\text{stat.}) \pm 128 (\text{syst.}).$$

The observed number of events in our signal region is 617.

Background Source	Number	Statistical Uncertainty	Systematic Uncertainty
γb	291	7	50
γc	92	25	45
Fake b, real γ	141	6	30
Fake γ	113	49	54
Total	637	54	128

TABLE III: Number of predicted background events in the signal region.

Figure 6 shows the distribution of $E_T(\gamma)$ in data with the background prediction overlaid.

Figure 7 shows the distribution of $E_T(b)$ in data with the background prediction overlaid.

Figure 8 shows the distribution of $E_T(j_2)$, where j_2 refers to the untagged jet in the event, in data with the background prediction overlaid.

Figure 9 shows the distribution of \cancel{E}_T after the application of \cancel{E}_T cleanup cuts but before the application of the $\cancel{E}_T > 25$ GeV cut in data with the background prediction overlaid.

Figure 10 shows the jet multiplicity distribution in data with the background prediction overlaid.

Figure 11 shows the distribution of the scalar sum of the transverse momenta of the γ , b -jet, 2nd jet, and \cancel{E}_T in data with the background prediction overlaid.

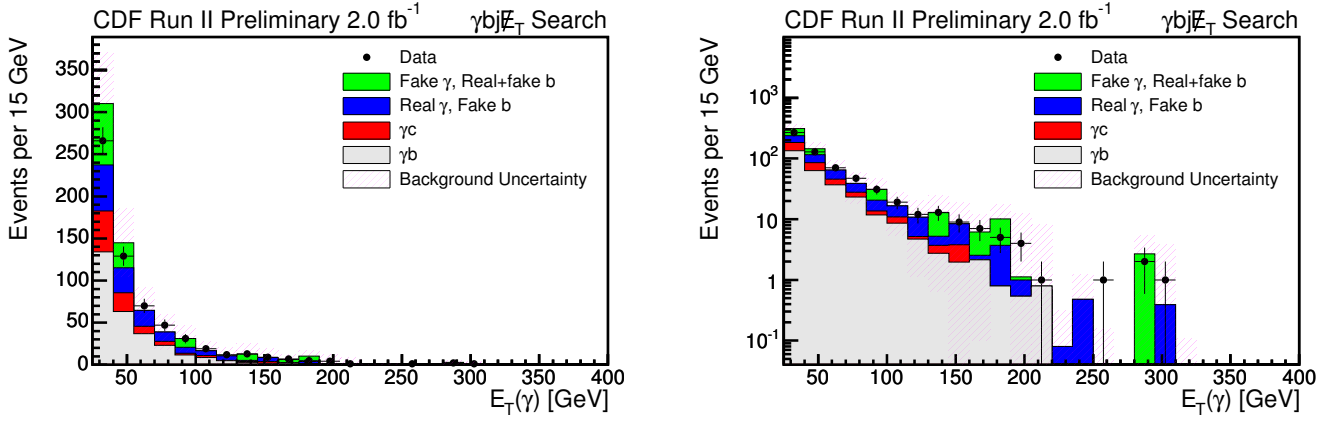


FIG. 6: $E_T(\gamma)$ distribution observed and background prediction in linear scale on the left and logarithmic scale on the right. The χ^2 per degree of freedom considering only Poisson errors on the data is 18/16.

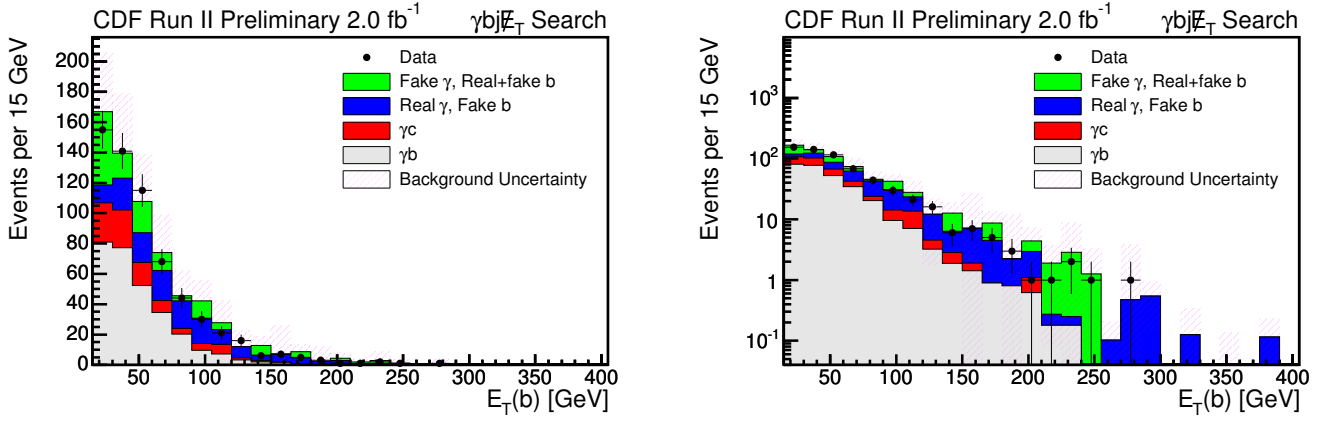


FIG. 7: $E_T(b)$ distribution observed and background prediction in linear scale on the left and logarithmic scale on the right. The χ^2 per degree of freedom considering only Poisson errors on the data is 57/16.

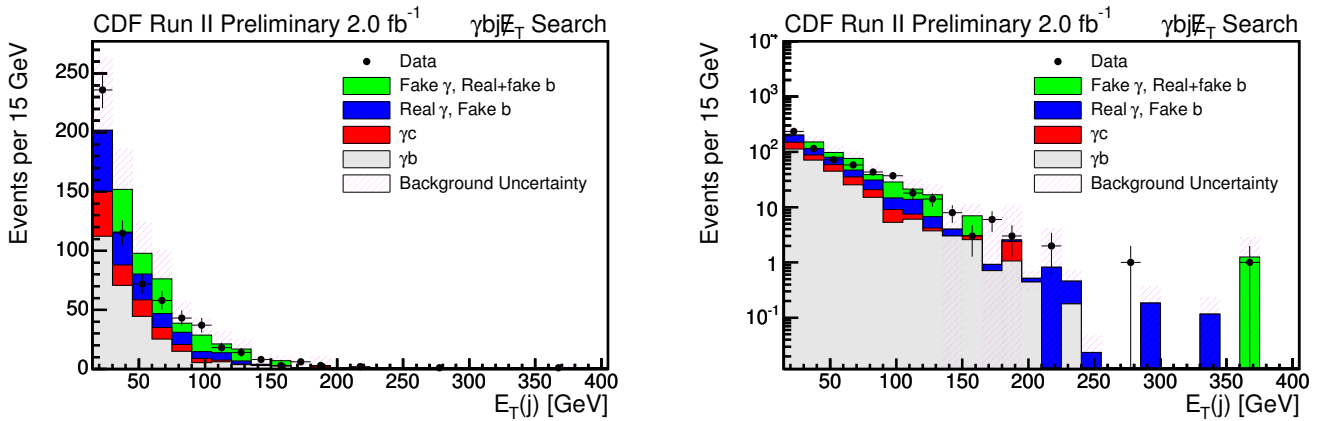


FIG. 8: $E_T(j_2)$, where j_2 refers to the untagged jet, distribution observed and background prediction in linear scale on the left and logarithmic scale on the right. The χ^2 per degree of freedom considering only Poisson errors on the data is 68/15.

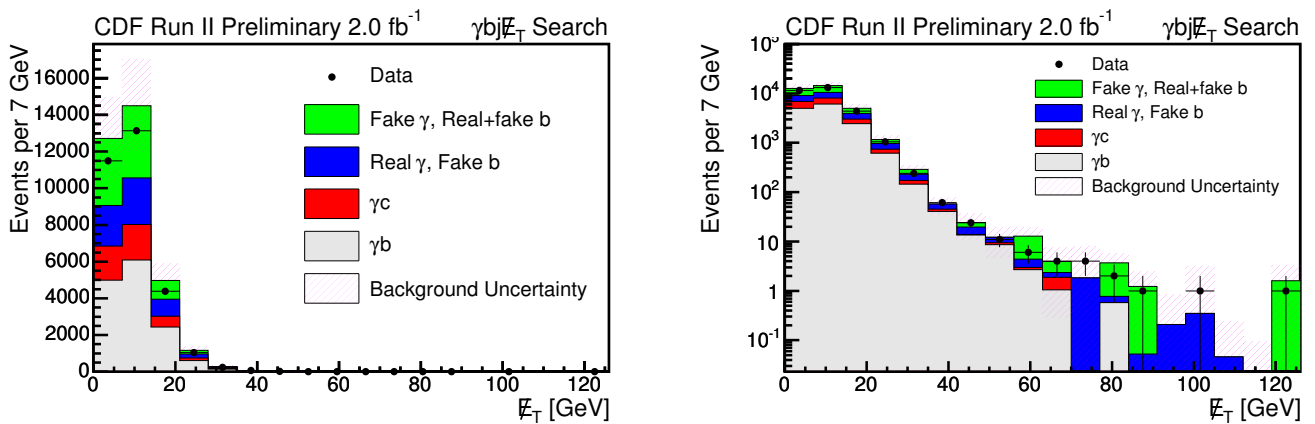


FIG. 9: The \cancel{E}_T distribution observed and background prediction in linear scale on the left and logarithmic scale on the right. The bin width is fixed at 7 GeV. The χ^2 per degree of freedom considering only Poisson errors on the data is 388/15.

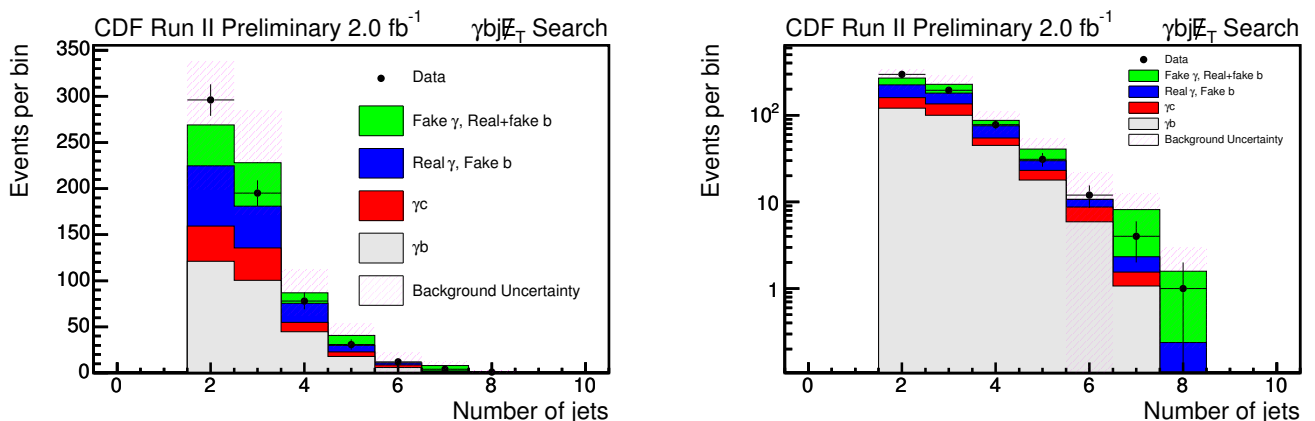


FIG. 10: Jet multiplicity distribution observed and background prediction in linear scale on the left and logarithmic scale on the right. The χ^2 per degree of freedom considering only Poisson errors on the data is 17/7.

Figure 12 shows the distribution of the scalar sum of the transverse momenta of the γ , \cancel{E}_T , and all jets in the event in data with the background prediction overlaid.

Figure 13 shows the distribution of the two-body mass of the photon+ b -jet, $M(\gamma b)$, in data with the background prediction overlaid.

Figure 14 shows the dijet mass distribution in data with the background overlaid.

Figure 15 shows the distribution of the transverse mass of the photon and \cancel{E}_T , $M^T(\gamma \cancel{E}_T)$, in data with the background distribution overlaid.

Figure 16 shows the distribution of the transverse mass of the dijet and \cancel{E}_T , $M^T(bj \cancel{E}_T)$, in data with the background distribution overlaid.

Figure 17 shows the three-body invariant mass distribution of the photon + b -jet + 2^{nd} jet, $M(\gamma bj)$, in data with the background prediction overlaid.

Figure 18 shows the observed dijet mass, $M(bj)$, versus the three-body invariant mass distribution of the photon + b -jet + 2^{nd} jet, $M(\gamma bj)$, in data.

VII. CONCLUSIONS

No structure peaking strongly over the background prediction is observed in any of the kinematic distributions studied. Furthermore, the number of events observed in data is consistent with the number of events expected from the Standard Model background prediction. We conclude that the 2 fb^{-1} $\gamma + b + j + \cancel{E}_T + X$ sample is consistent with Standard Model background expectations.

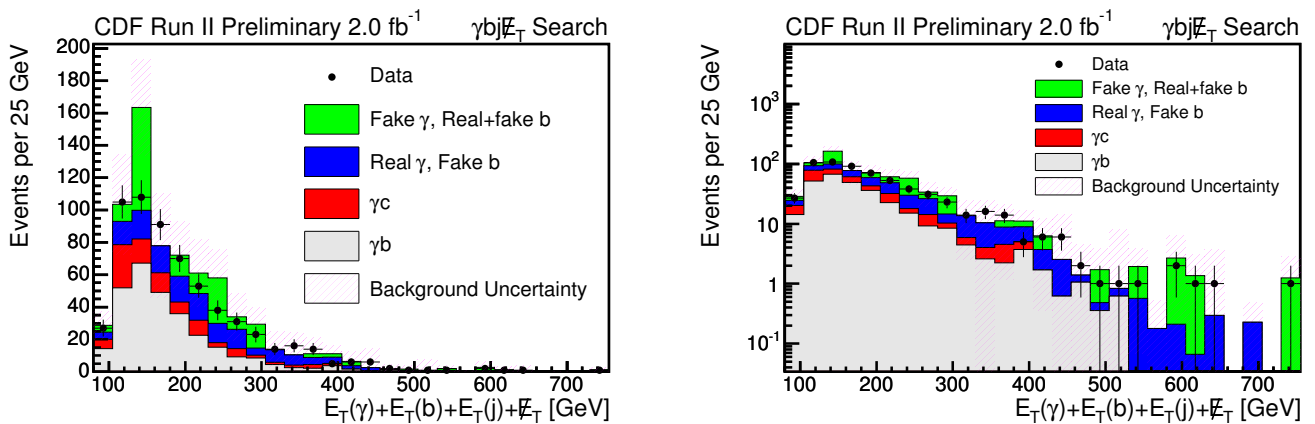


FIG. 11: Distribution of the scalar sum of the transverse momenta of the γ , b-jet, 2^{nd} jet, and \cancel{E}_T observed and background prediction in linear scale on the left and logarithmic scale on the right. The bin width is fixed at 25 GeV. The χ^2 per degree of freedom considering only Poisson errors on the data is 59/23.

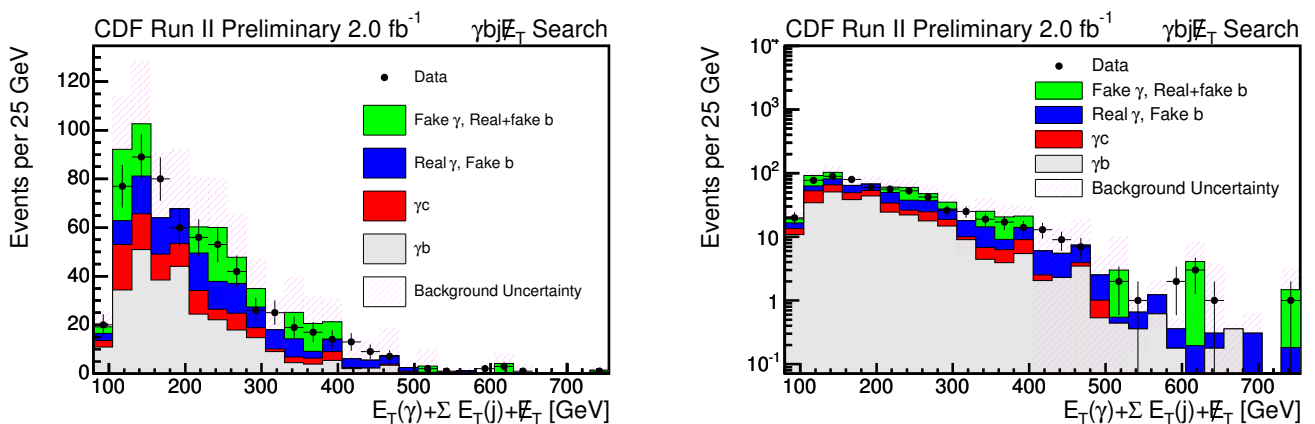


FIG. 12: Distribution of the scalar sum of the transverse momenta of the γ , all jets in the event, and \cancel{E}_T observed and background prediction in linear scale on the left and logarithmic scale on the right. The bin width is fixed at 25 GeV. The χ^2 per degree of freedom considering only Poisson errors on the data is 31/22.

Acknowledgments

We thank the Fermilab staff and the technical staffs of the participating institutions for their vital contributions. This work was supported by the U.S. Department of Energy and National Science Foundation; the Italian Istituto Nazionale di Fisica Nucleare; the Ministry of Education, Culture, Sports, Science and Technology of Japan; the Natural Sciences and Engineering Research Council of Canada; the National Science Council of the Republic of China; the Swiss National Science Foundation; the A.P. Sloan Foundation; the Bundesministerium fuer Bildung und Forschung, Germany; the Korean Science and Engineering Foundation and the Korean Research Foundation; the Particle Physics and Astronomy Research Council and the Royal Society, UK; the Russian Foundation for Basic Research; the Comision Interministerial de Ciencia y Tecnologia, Spain; and in part by the European Community's Human Potential Programme under contract HPRN-CT-20002, Probe for New Physics.

-
- [1] S. Ambrosanio, G. L. Kane, G. D. Kribs, S. P. Martin, and S. Mrenna, Phys. Rev. Lett. **76**, 3498 (1996); G. L. Kane and S. Mrenna, Phys. Rev. Lett. **77** 3502 (1996); S. Ambrosanio, G. L. Kane, G. D. Kribs, S. P. Martin, and S. Mrenna, Phys. Rev. D **55**, 1372 (1997).
 [2] F. Abe *et al.* (CDF Collaboration), Phys. Rev. D **59**, 092002 (1999); F. Abe *et al.* (CDF Collaboration), Phys. Rev. Lett.

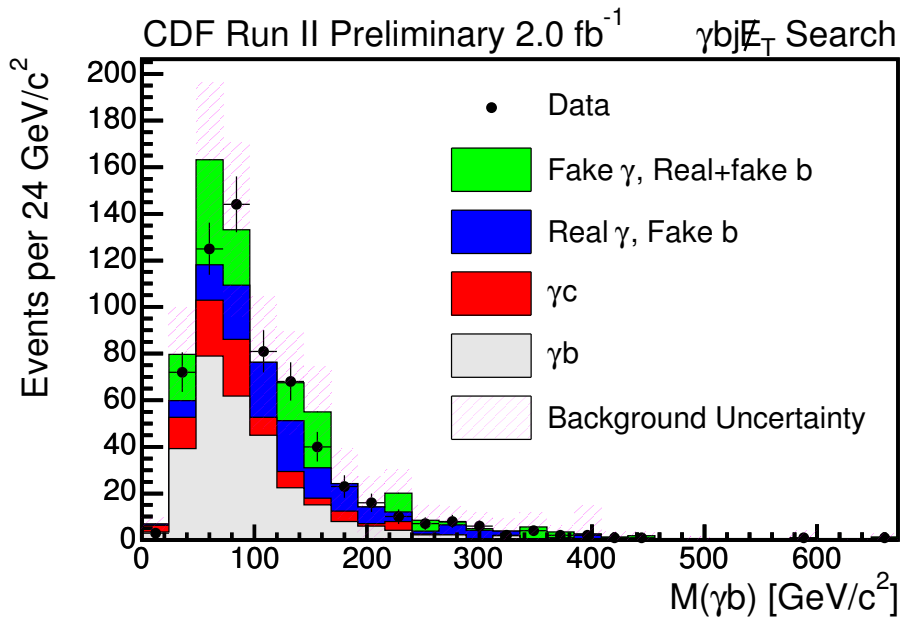


FIG. 13: Distribution of the mass of the photon + b-jet, $M(\gamma b)$, observed and background prediction. The bin width is fixed at $24 \text{ GeV}/c^2$. The χ^2 per degree of freedom considering only Poisson errors on the data is $40/21$.

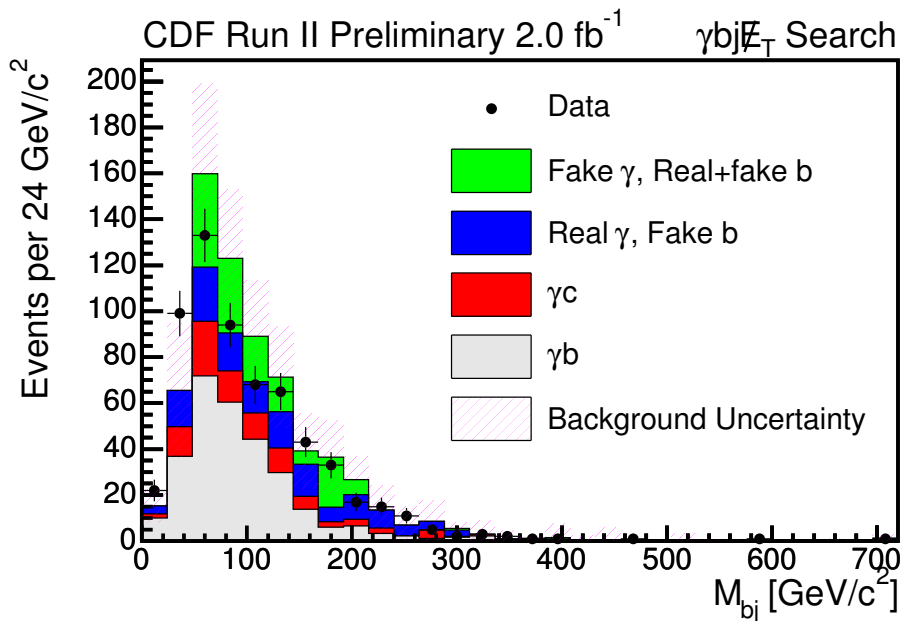


FIG. 14: Dijet mass distribution, $M(bj)$, observed and background prediction. The bin width is fixed at $24 \text{ GeV}/c^2$. The χ^2 per degree of freedom considering only Poisson errors on the data is $54/20$.

81, 1791 (1998); D. Toback, Ph.D. thesis, University of Chicago, 1997.

[3] K. Lane, “Search for low-scale technicolor at the Tevatron,” arXiv:hep-ph/0605119.

[4] E. Eichten and K. Lane, “Low-scale technicolor at the Tevatron and LHC,” arXiv:0706.2339 [hep-ph].

[5] A. R. Zerwekh, C. O. Dib and R. Rosenfeld, Phys. Rev. D **75**, 097702 (2007) [arXiv:hep-ph/0702167].

[6] F. Abe, *et al.*, Nucl. Instrum. Methods Phys. Res. A **271**, 387 (1988); D. Amidei, *et al.*, Nucl. Instrum. Methods Phys. Res. A **350**, 73 (1994); F. Abe, *et al.*, Phys. Rev. D **52**, 4784 (1995); P. Azzi, *et al.*, Nucl. Instrum. Methods Phys. Res. A **360**,

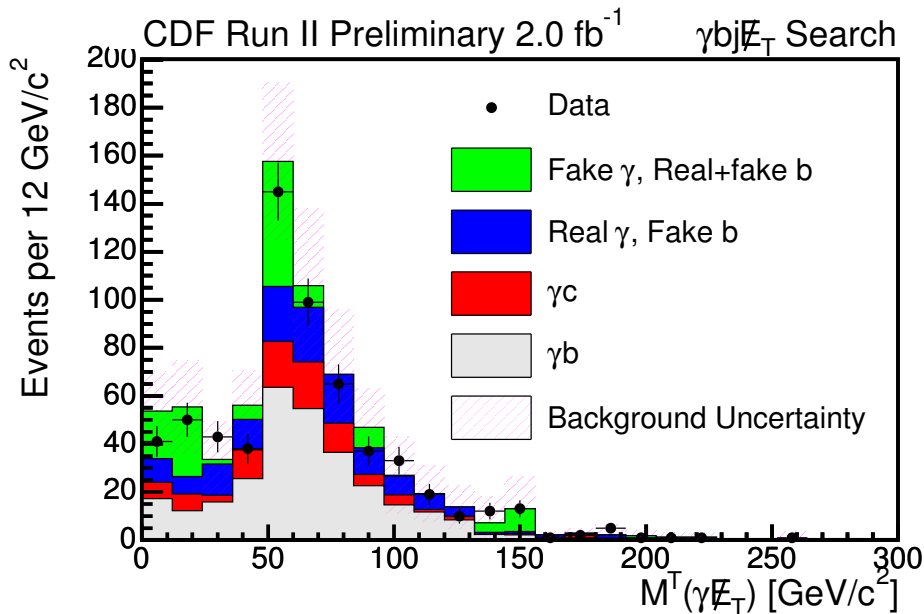


FIG. 15: Transverse mass distribution of the photon + \cancel{E}_T , $M^T(\gamma\cancel{E}_T)$, observed and background prediction. The χ^2 per degree of freedom considering only Poisson errors on the data is 29/20.

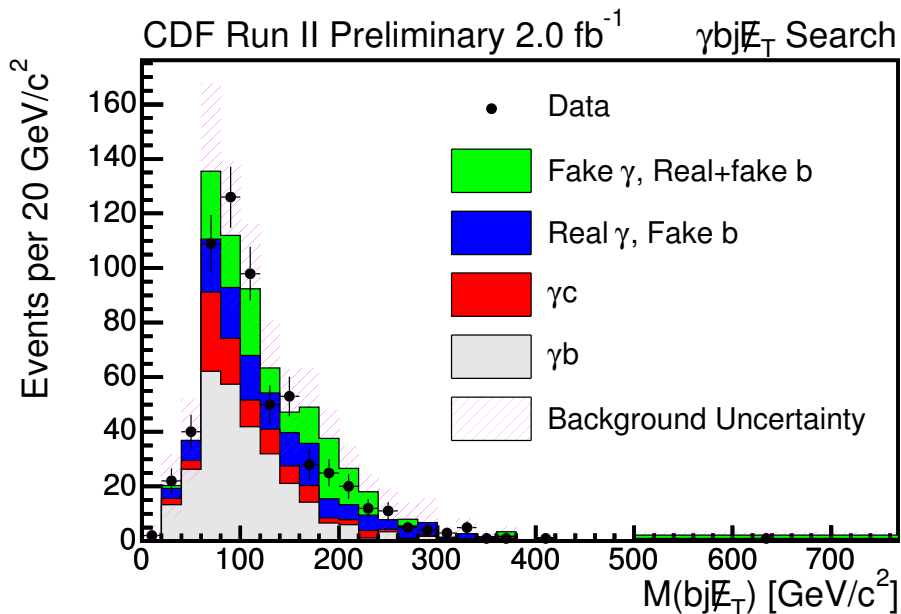


FIG. 16: Transverse mass distribution of the dijet + \cancel{E}_T , $M^T(bj\cancel{E}_T)$, observed and background prediction using variable bins to show all the overflows. The χ^2 per degree of freedom considering only Poisson errors on the data is 56/21.

137 (1995); The CDFII Detector Technical Design Report, Fermilab-Pub-96/390-E.

[7] CDF Collaboration, “Measurement of the $t\bar{t}$ production cross section in $p\bar{p}$ collisions at $\sqrt{s} = 1.96$ TeV using Lepton+Jet Events with Secondary Vertex b -Tagging,” CDF Note 8795 (2007) [http://www-cdf.fnal.gov/physics/new/top/confNotes/cdf8795_SecVtxXSPublic.ps].

[8] J. Alwall, P. Demin, S. de Visscher, R. Frederix, M. Herquet, F. Maltoni, T. Plehn, D. .L. Rainwater, T. Stelzer, “*Mad-Graph/MadEvent v4: The New Web Generator*”, JHEP **09**, 028 (2007).

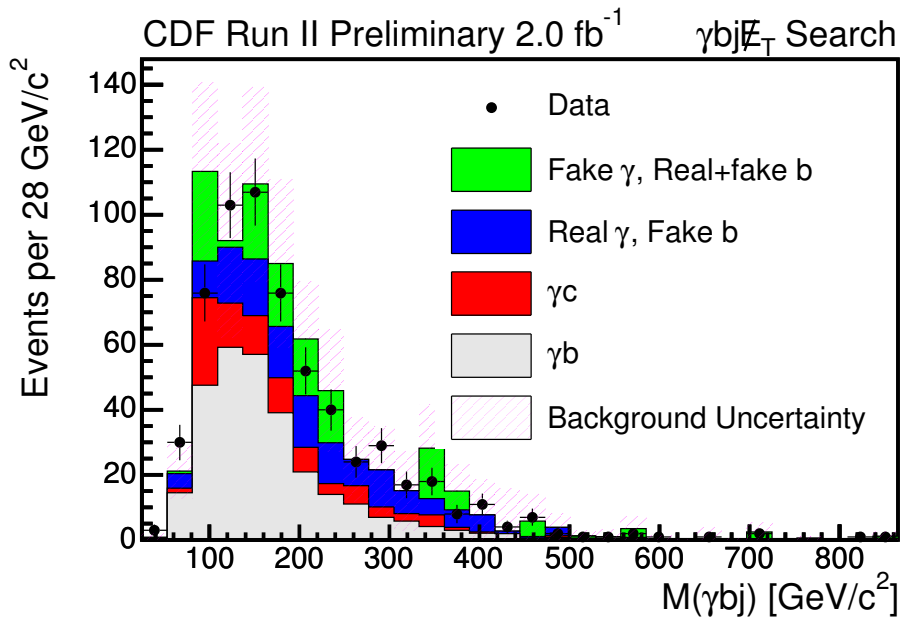


FIG. 17: Three-body invariant mass distribution, $M(\gamma bj)$, observed and background prediction using variable bins to show all the overflows. The bin width is fixed at $28 \text{ GeV}/c^2$. The χ^2 per degree of freedom considering only Poisson errors on the data is $48/25$.

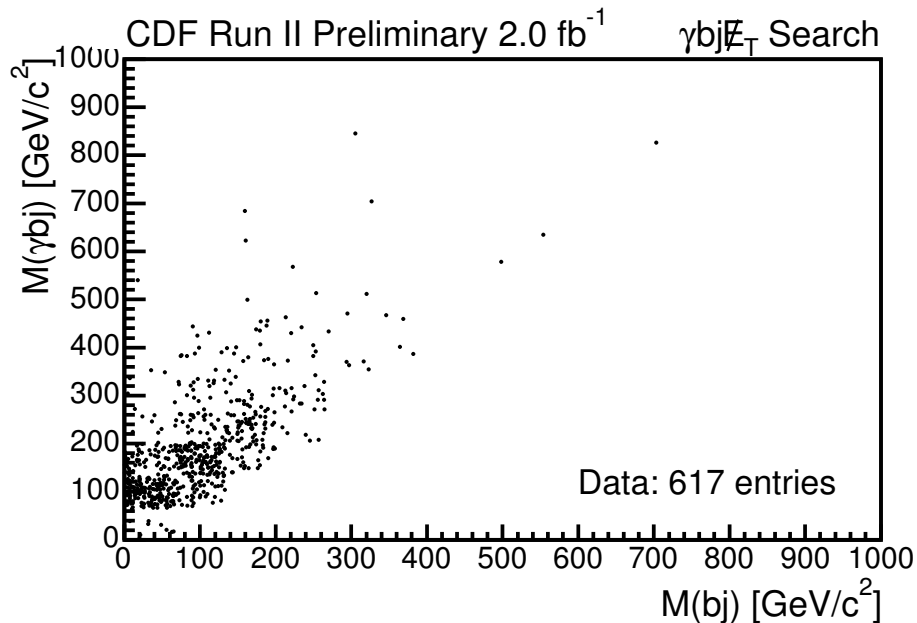


FIG. 18: Observed dijet mass, $M(bj)$, versus three-body invariant mass distribution, $M(\gamma bj)$.

- [9] T. Sjostrand, S. Mrenna, P. Skands, "PYTHIA 6.4 Physics and Manual", JHEP **05**, 026 (2006).
- [10] J. Alwall, *et al.*, "Comparative study of various algorithms for the merging of parton showers and matrix elements in hadronic collisions", arXiv:0706.2569v2 [hep-ph].
- [11] F. Abe, *et al.*, (CDF Collaboration), "A Prompt photon cross-section measurement in anti-p p collisions at $\sqrt{s} = 1.8 \text{ TeV}$." Phys. Rev. D **48**, 2998 (1993).
- [12] W. Verkerke and D. Kirkby (2003). For documentation and source code, see <http://roofit.sourceforge.net> and

arXiv:physics/0306116 [physics.data-an].